Journal of Applied Electrochemistry (2007) 37:421–427
DOI 10.1007/s10800-006-9273-1

Variation of $LiNiO_2$ cathode properties with substitution of Ga, In and Tl by the combustion method

MYOUNGYOUP SONG[1,*], SUNGNAM KWON[1], IKHYUN KWON[1] and HYERYOUNG PARK[2]
[1]*Division of Advanced Materials Engineering, Research Center for Advanced Materials Development, Engineering Research Institute, Chonbuk National University, 664-14 1ga Deogjindong Deogjingu, Jeonju, 561-756, Republic of Korea*
[2]*Faculty of Applied Chemical Engineering, Chonnam National University, 300Yongbongdong Bukgu, Gwangju, 500-757, Republic of Korea*
*(*author for correspondence, tel.: + 82-63-270-2379, fax: + 82-63-270-2386, e-mail: songmy@chonbuk.ac.kr)*

Received 2 February 2006; accepted in revised form 24 October 2006

Key words: $LiNi_{1-y}M_yO_2$ (M = Ga, In and Tl), substitution of elements, combustion method, I_{003}/I_{104}, *R*-factor, cation mixing

Abstract

$LiNi_{1-y}M_yO_2$ (M = Ga, In and Tl, y = 0.010, 0.025 and 0.050) with small y were synthesized by the combustion method by calcining in an O_2 stream at 750 °C for 36 h. XRD analyses, SEM observation and measurement of the variation of discharge capacity with the number of cycles were carried out. All the samples had the $R\bar{3}m$ structure and $LiNi_{1-y}In_yO_2$ contained $LiInO_2$ phase as an impurity. Among $LiNi_{1-y}Ga_yO_2$ the sample with y = 0.025 had a relatively large first discharge capacity (172.2 mAh g^{-1}) and relatively good cycling performance (discharge capacity 140.3 mAh g^{-1} at n = 20). For $LiNi_{0.975}M_{0.025}O_2$ (M = Ga, In and Tl), the first discharge capacity decreased in the order of the substituted element Ga, In and Tl. The variations of cation mixing and hexagonal ordering with the substituted element (decrease in I_{003}/I_{104} and increase in *R*-factor from M = Ga through M = Tl) are considered to lead to the behavior of the first discharge capacity with the substituted element. $LiNi_{0.975}Tl_{0.025}O_2$ had the smallest degradation rate of the discharge capacity.

1. Introduction

The transition metal oxides such as $LiMn_2O_4$ [1–3], $LiCoO_2$ [4–6] and $LiNiO_2$ [7–16] have been investigated as cathode materials for lithium secondary batteries. $LiMn_2O_4$ is very cheap and does not bring about environmental pollution, but its cycling performance is not good. $LiCoO_2$ has a large diffusivity and a high operating voltage, and it can be easily prepared. However, it has a disadvantage that it contains an expensive element Co. $LiNiO_2$ is a very promising cathode material since it has a large discharge capacity and is relatively excellent from the viewpoints of economics and environment. However, its preparation is very difficult as compared with $LiCoO_2$ and $LiMn_2O_4$.

It is known that $Li_{1-x}Ni_{1+x}O_2$ forms rather than stoichiometric $LiNiO_2$ during preparation. This phenomenon is called cation mixing. Excess nickel occupies the Li sites, destroying the ideally layered structure and preventing lithium ions from easy movement for intercalation and deintercalation during cycling. This results in a small discharge capacity and a poor cycling performance.

To improve the electrochemical properties of $LiNiO_2$, Co [17–21], Al [22–25], Ti [26–30], Ga [31], Mn [32] and Fe [33–36] ions were substituted for lithium ion. Rougier et al. [18] reported that the stabilization of the two-dimensional character of the structure by cobalt substitution in $LiNiO_2$ is correlated with an increase in the cell performance due to the decrease in the amount of extra-nickel ions in the inter-slab space which impede the lithium diffusion. Guildmard et al. [22] investigated the electrochemical performances of $LiNi_{1-y}Al_yO_2$ ($0.10 \le y \le 0.50$) synthesized by a co-precipitation method. They showed that aluminum substitution suppressed all the phase transitions observed for the $LiNiO_2$ system. According to Gao et al. [27] and Kim et al. [29, 30], the substitution of Ti for Ni resulted in a large discharge capacity and a good cycling performance. Chang et al. [27] detected partial disordering between transition metal (Ni and Ti) layer and lithium by the Rietveld refinement in $Li_xNi_{1-y}Ti_yO_2$ ($0.1 \le y \le 0.5$) prepared by solid state reaction. By considering the ionic radius and the Ni–O bond length, the Ni(II) ions are concluded to be partially stabilized in the lithium site. Nishida et al. [31] reported that

gallium–doping to $LiNiO_2$ stabilizes the crystal structure during the charging process and leads to better cycling performance than $LiNiO_2$. Guildmard et al. [32] reported the presence of 5 or 3% extra nickel ions in the inter-slab space, respectively, in two types of $LiNi_{0.90}Mn_{0.10}O_2$ synthesized by a co-precipitation method in the presence of either 5 or 50% lithium excess. Cycling tests showed a decrease in the electrochemical properties with a large irreversible capacity at the end of the first cycle, in comparison with $LiNiO_2$. Reimers et al. [34] studied the solid solution series $LiFe_yNi_{1-y}O_2$ ($0.1 \leq y \leq 0.5$). They reported that the cation mixing was primarily between Fe and Li, and the amount of Li which can be reversibly cycled decreases as y increases. Kanno et al. [35] synthesized $LiFe_{1-y}Ni_yO_2$ by ion-exchange reaction and reported that cycling capacities of the 4 V region decreased with increase in iron content. Prado et al. [36] studied cation distribution in the $Li_{1-Z}(Ni_{1-y}Fe_y)_{1+z}O_2$ electrode materials, and reported that for the largest y and z values iron ions are simultaneously present in the slab and in the inter-slab space.

$LiNiO_2$ synthesized by the solid-state reaction method does not have large discharge capacity and does not exhibit good cycling performance, probably because it has poor crystallinity and non-homogeneous particle size. On the other hand, homogeneous mixing of starting materials is possible by the combustion method because nitrates as starting materials and urea as a fuel are mixed in distilled water by a magnetic stirrer. This may lead to good crystallinity and homogeneous particle size when the sample is synthesized.

Based on the field of propellants and explosives, combustion synthesis is a chemical reaction between the metal salts and suitable organic fuel. The reaction accompanies an exothermic and self-sustaining chemical reaction [37]. Its processing feature is that the initial heat is required to start the chemical reaction. Subsequently, the chemical reaction supplies the energy to react the materials itself without external energy [38].

The range of substituted fraction y in $LiNi_{1-y}M_yO_2$ of many researches was $0.0 \leq y \leq 0.9$. The results of these researches showed that charge and discharge capacities decreased rapidly when $y > 0.025$ except for Co substitution.

In this work samples were synthesized by the combustion method. Ni in $LiNiO_2$ was substituted by Ga, In and Tl. The ionic radii of Ga, In and Tl are 0.62, 0.79 and 0.88 Å, respectively. We chose $0.010 \leq y \leq 0.050$ as the range of y, in which y are much smaller than the substituted fractions of the reported results. The electrochemical properties of the synthesized samples were then investigated.

2. Experimental

The optimum conditions to synthesize $LiNiO_2$ by the combustion method, studied in our previous work [16], were preheating at 400 °C for 30 min in air and calcination at 750 °C for 36 h in an O_2 stream. $LiNi_{1-y}M_yO_2$ (M = Ga, In and Tl, $y = 0.010$, 0.025 and 0.050) were synthesized under these conditions. Lithium nitrate ($LiNO_3$, Aldrich Chemical), nickel hexahydrate ($Ni(NO_3)_2{\cdot}6H_2O$, Aldrich Chemical), $GaNO_3{\cdot}XH_2O$ (Aldrich Chemical, 99.999%) or $In(NO_3)_3{\cdot}5H_2O$ (Aldrich Chemical, 99.99%) or $TlNO_3$ (Aldrich Chemical, 99.9%) were used as starting materials. The starting materials, in the desired proportions, were mixed with urea by a magnetic stirrer. The mole ratio of urea to nitrate was 3.6. The heating rate and the cooling rate were about 100 °C h^{-1}.

The phase identification of the synthesized samples was carried out by X-ray diffraction analysis using CuK_α radiation. A Rigaku III/A X-ray diffractometer was used. The scanning rate was 6° min^{-1} and the scanning range of diffraction angel (2θ) was $10° \leq 2\theta \leq 80°$. The morphologies of the samples were observed by scanning electron microscopy (SEM).

To measure the electrochemical properties, the electrochemical cells consisted of the prepared sample as a positive electrode, Li metal as a negative electrode and an electrolyte of 1 M $LiPF_6$ in a 1:1 (volume ratio) mixture of ethylene carbonate (EC) and diethyl carbonate (DEC). A Whatman glass fiber was used as a separator. The cells were assembled in an argon-filled dry box. To fabricate the positive electrode, active material, acetylene black and polyvinylidene fluoride (PVDF) binder dissolved in N-methyl-2-pyrrolidone (NMP) were mixed in a weight ratio 85:10:5 and applied on Al foil. All the electrochemical tests were performed at room temperature with a battery charge-discharge cycle tester at 0.1 C in a potential range from 2.7 to 4.4 V.

3. Results and discussion

Figure 1 shows X-ray powder diffraction (XRD) patterns of $LiNi_{1-y}Ga_yO_2$ ($y = 0.010$, 0.025 and 0.050) calcined at 750 °C for 36 h. All the samples have the α-$NaFeO_2$ structure of the rhombohedral system (space group; $R\bar{3}m$) with no evidence of impurity. The $R\bar{3}m$ structure is distorted in the c-axis direction of the hexagonal structure. This is reflected by the split of the 006 and 102 peaks, and of the 108 and 110 peaks in the XRD patterns. The 006 and 102 peaks were not split, but the 108 and 110 peaks were split for all the samples.

Ohzuku et al. [39] reported that the electrochemically reactive $LiNiO_2$ showed larger integrated intensity ratio of 003 peak to 104 peak (I_{003}/I_{104}) and a clear split of the 108 and 110 peaks in their XRD patterns. The degree of cation mixing (displacement of nickel and lithium ions) is low if the value of I_{003}/I_{104} is large and the 108 and 110 peaks are split clearly. The value of $(I_{006}+I_{102})/I_{101}$, called the *R*-factor, is known to be smaller as the unit cell volume of $Li_yNi_{2-y}O_2$ gets smaller. The *R*-factor increases as y in $Li_yNi_{2-y}O_2$ decreases for y near 1. This indicates that the *R*-factor

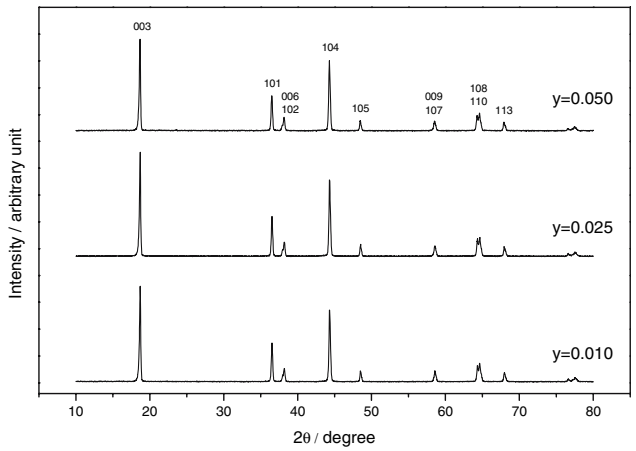

Fig. 1. XRD patterns of $LiNi_{1-y}Ga_yO_2$ (y = 0.010, 0.025 and 0.050) calcined at 750 °C for 36 h.

Table 1. Data calculated from XRD patterns of $LiNi_{1-y}Ga_yO_2$ (y = 0.010, 0.025 and 0.050) calcined at 750 °C for 36 h

	a/Å	c/Å	c/a	I_{003}/I_{104}	*R*-factor	Unit cell volume/Å^3
y = 0.010	2.881	14.213	4.933	1.334	0.513	102.167
y = 0.025	2.881	14.218	4.935	1.366	0.509	102.209
y = 0.050	2.883	14.221	4.932	1.308	0.526	102.380

increases as the degree of cation mixing becomes larger [7].

The cation mixing in layered materials makes sliding between basal planes impossible, resulting in electrochemical inactivity [39]. Hexagonal ordering implies good layered structure which has a characteristic property of sliding between basal planes. High cation mixing thus corresponds to low hexagonal ordering. A Large *R*-factor, which increases with the degree of cation mixing, indicates low hexagonal ordering.

Table 1 gives the lattice parameters a, c, c/a, I_{003}/I_{104}, *R*-factor and unit cell volume calculated from XRD patterns of $LiNi_{1-y}Ga_yO_2$ (y = 0.010, 0.025 and 0.050) calcined at 750 °C for 36 h. The sample with y = 0.025 has the largest I_{003}/I_{104}, the smallest value of *R*-factor and a medium value of unit cell volume.

Figure 2 shows the SEM photographs of $LiNi_{1-y}Ga_yO_2$ (y = 0.010, 0.025 and 0.050) calcined at 750 °C for 36 h. The samples contain agglomerated particles and relatively small particles on the agglomerates. The particles of the agglomerates grow slightly as the value of y increases. Particle size and shape of relatively small particles on the agglomerates are similar for all the compositions.

Figure 3 shows the variations of the discharge capacity at 0.1 C of $LiNi_{1-y}Ga_yO_2$ (y = 0.010, 0.025 and 0.050) calcined at 750 °C for 36 h. The sample with y = 0.010 has the largest first discharge capacity (176.5 mAh g^{-1}). The sample with y = 0.025 has the smallest first discharge capacity (172.2 mAh g^{-1}), but it has the largest discharge capacity from n = 2 through n = 17. This is considered to be related to the largest I_{003}/I_{104} and the smallest value of *R*-factor of this sample.

Figure 4 shows XRD patterns of $LiNi_{1-y}In_yO_2$ (y = 0.010, 0.025 and 0.050) calcined at 750 °C for 36 h. All the samples have the phase with $R\bar{3}m$ structure. In addition, they show peaks for $LiInO_2$, and its fraction increases with the value of y.

Table 2 gives the lattice parameters a, c, c/a, I_{003}/I_{104}, *R*-factor and unit cell volume calculated from the XRD patterns of $LiNi_{1-y}In_yO_2$ (y = 0.010, 0.025 and 0.050) calcined at 750 °C for 36 h. The sample with y = 0.010 has the largest I_{003}/I_{104}, the smallest value of *R*-factor and the smallest unit cell volume.

Fig. 5 shows the SEM photographs of $LiNi_{1-y}In_yO_2$ (y = 0.010, 0.025 and 0.050) calcined at 750 °C for 36 h. The samples contain agglomerated particles and relatively small particles on the agglomerates. The sizes of the particles in the agglomerates and the relatively small particles on the agglomerates increase with increase in the value of y and then decrease. The sample with y = 0.050 has the smallest particles.

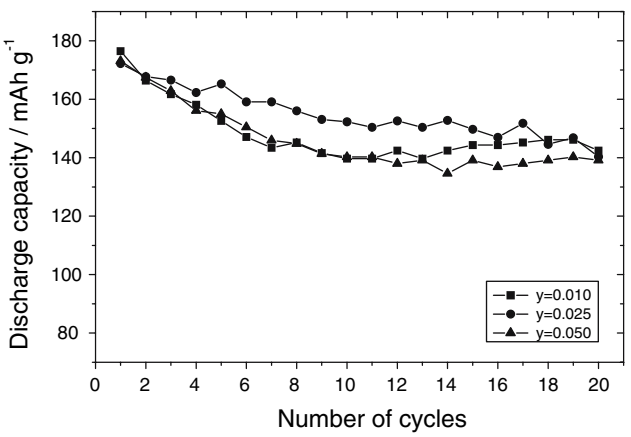

Fig. 3. Variations of discharge capacity at 0.1 C with the number of cycles for $LiNi_{1-y}Ga_yO_2$ synthesized by the combustion method.

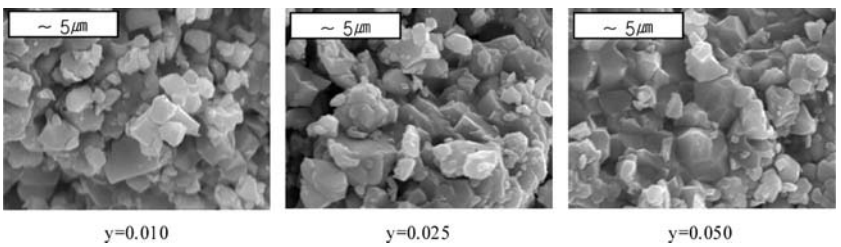

Fig. 2. SEM photographs of $LiNi_{1-y}Ga_yO_2$ (y = 0.010, 0.025 and 0.050) calcined at 750 °C for 36 h.

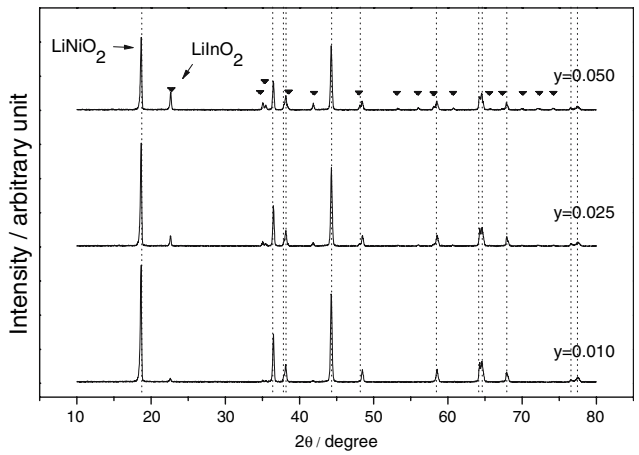

Fig. 4. XRD patterns of $LiNi_{1-y}In_yO_2$ (y = 0.010, 0.025 and 0.050) calcined at 750 °C for 36 h.

Table 2. Data calculated from XRD patters of $LiNi_{1-y}In_yO_2$ (y = 0.010, 0.025 and 0.050) calcined at 750 °C for 36 h

	a/Å	c/Å	c/a	I_{003}/I_{104}	*R*-factor	Unit cell volume/Å^3
y = 0.010	2.883	14.223	4.933	1.326	0.506	102.396
y = 0.025	2.880	14.377	4.992	1.317	0.531	103.284
y = 0.050	2.885	14.240	4.936	1.135	0.554	102.645

Figure 6 shows the variations of the discharge capacity at 0.1 C of $LiNi_{1-y}In_yO_2$ (y = 0.010, 0.025 and 0.050) calcined at 750 °C for 36 h. The sample with y = 0.010 has the largest first discharge capacity (167.7 mAh g^{-1}), and the first discharge capacity decreases with increase in y. The sample with y = 0.010 has the largest discharge capacity from n = 1 through n = 20 and has the discharge capacity 136.6 mAh g^{-1} at n = 20. This is considered to be related to the largest I_{003}/I_{104}, the smallest value of *R*-factor and the smallest unit cell volume of this sample.

Figure 7 shows the X-ray powder diffraction (XRD) patterns of $LiNi_{1-y}Tl_yO_2$ (y = 0.010, 0.025 and 0.050) calcined at 750 °C for 36 h. All the samples have only the phase with $R\bar{3}m$ structure and do not exhibit impurity peaks.

Table 3 gives the lattice parameters a, c, c/a, I_{003}/I_{104}, *R*-factor and unit cell volume calculated from XRD patterns of $LiNi_{1-y}Tl_yO_2$ (y = 0.010, 0.025 and 0.050) calcined at 750 °C for 36 h. The sample with y = 0.050 has the largest I_{003}/I_{104} and the smallest value of *R*-factor. The sample with y = 0.025 has a medium value of I_{003}/I_{104}, nearly the smallest value of *R*-factor and the smallest unit cell volume.

Figure 8 shows the SEM photographs of $LiNi_{1-y}Tl_yO_2$ (y = 0.010, 0.025 and 0.050) calcined at 750 °C for 36 h. The samples contain agglomerated particles and relatively small particles on the agglomerates. The sizes of the particles in the agglomerates and relatively small particles on the agglomerates increase with increase in the value of y.

Figure 9 shows the variations of the discharge capacity at 0.1 C of $LiNi_{1-y}Tl_yO_2$ (y = 0.010, 0.025 and 0.050) calcined at 750 °C for 36 h. The sample with

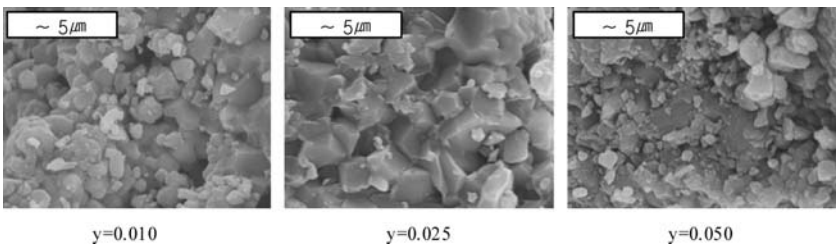

Fig. 5. SEM photographs of $LiNi_{1-y}In_yO_2$ (y = 0.01, 0.025 and 0.05) calcined at 750 °C for 36 h.

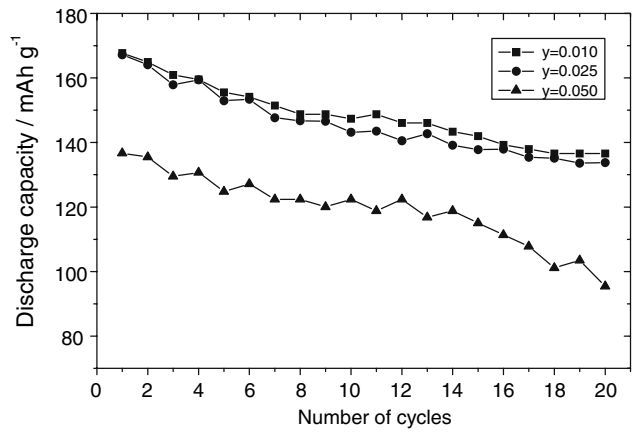

Fig. 6. Variations of discharge capacity at 0.1 C with the number of cycles for $LiNi_{1-y}In_yO_2$ synthesized by the combustion method.

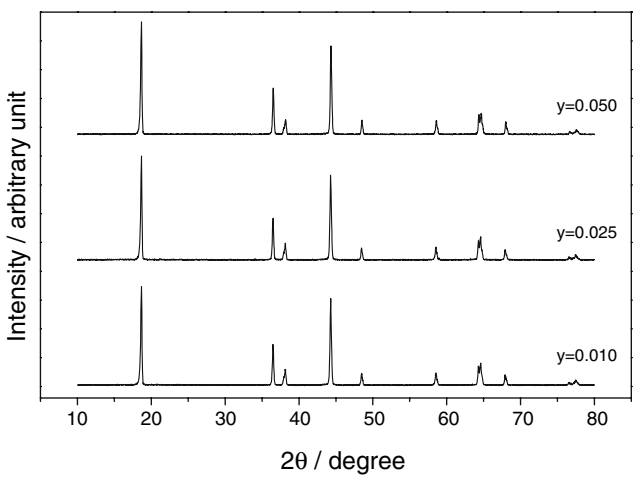

Fig. 7. XRD patterns of $LiNi_{1-y}Tl_yO_2$ (y = 0.01, 0.025 and 0.05) calcined at 750 °C for 36 h.

Table 3. Data calculated from XRD patters of $LiNi_{1-y}Tl_yO_2$ (y = 0.01, 0.025 and 0.05) calcined at 750 °C for 36 h

	a/Å	c/Å	c/a	I_{003}/I_{104}	*R*-factor	Unit cell volume/Å^3
y = 0.010	2.883	14.238	4.938	1.137	0.646	102.512
y = 0.025	2.881	14.213	4.933	1.229	0.647	102.187
y = 0.050	2.877	14.380	5.000	1.275	0.512	103.060

y = 0.025 has the largest first discharge capacity (157.2 mAh g^{-1}). The samples with y = 0.010 and 0.050 have similar first discharge capacities. The sample with y = 0.025 has the largest discharge capacity from n = 1 through n = 20. It has a discharge capacity of 137.9 mAh g^{-1} at n = 20. This is probably related to nearly the smallest value of *R*-factor and the smallest unit cell volume of this sample. However, this sample has a medium value of I_{003}/I_{104}.

Figure 10 shows the – dQ/|dV| vs. voltage plot at the first cycle and the second cycle for $LiNi_{0.975}Ga_{0.025}O_2$ synthesized by the combustion method. During charge and discharge, $LiNiO_2$ goes through several phase transitions such as transition from hexagonal (H1) to monoclinic (M), to hexagonal (H2) and to hexagonal (H3) or vice versa [40–42]. In addition, it is reported that at the phase transition from H2 to H3, contraction of the lattice parameter c axis occurs and electrochemical properties become worse [42]. The sharp peak corresponds to a phase transition at which two phases coexist. The broad peak corresponds to a phase transition at which one-phase changes continuously [28]. The oxidation peaks at 3.76, 4.03 and 4.24 V for the first cycle are considered to correspond to transitions from H1 to M, from M to H2 and from H2 to H3, respectively. The peak for monoclinic phase (M) continuous phase transition seems to be hidden within the peak for the transition from H1 to M. The reduction peaks at 4.14, 3.96, 3.70 and 3.62 V for the first cycle are considered to correspond to transitions from H3 to H2 and from H2 to M, monoclinic phase (M) continuous phase transition, and transition from M to H1, respectively. The oxidation peaks and the reduction peaks for the second cycle appear more clearly than those for the first cycle. This is probably because the unstable sites were destroyed during de-intercalation and intercalation of the first cycle. The oxidation peak for monoclinic phase (M) continuous phase transition appears broadly around 3.77 V.

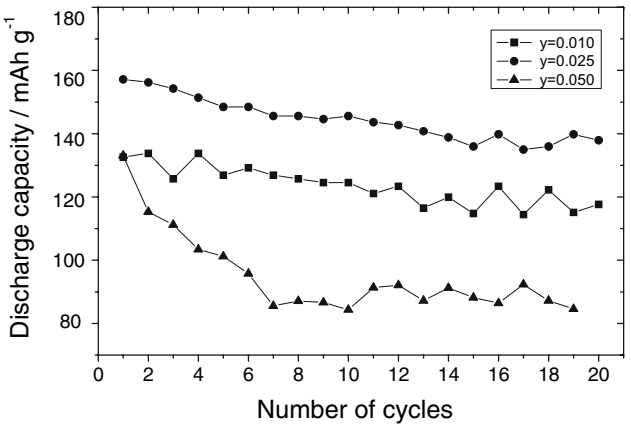

Fig. 9. Variations of discharge capacity at 0.1 C with the number of cycles for $LiNi_{1-y}Tl_yO_2$ synthesized by the combustion method.

The samples with y = 0.025 showed, roughly, better electrochemical properties than those with other values of y. Figure 11 shows the variations of the discharge capacity at 0.1 C with number of cycles of $LiNi_{0.975}M_{0.025}O_2$ (M = Ga, In and Tl) synthesized by the combustion method. $LiNi_{0.975}Ga_{0.025}O_2$ has the largest first discharge capacity and relatively good cycling performance.

Figure 12 shows the variations with the substituted element of (a) the first discharge capacity, (b) the degradation rate of discharge capacity, (c) I_{003}/I_{104} and (d) *R*-factor for $LiNi_{0.975}M_{0.025}O_2$ (M = Ga, In, and Tl) synthesized by the combustion method. As the substituted elements vary from Ga to In and then to Tl, the first discharge capacity and I_{003}/I_{104} decrease and the *R*-factor increases. The degradation rate of discharge capacity has a maximum value when the substituted element is In. The variation trend of the first discharge capacity with the substituted element is similar to that of I_{003}/I_{104}. The large value of I_{003}/I_{104} indicates low cation mixing. The decrease in I_{003}/I_{104} from M = Ga through M = Tl is considered to lead to the decrease in the first discharge capacity from Ga through Tl substitution. The variation of the first discharge capacity with the substituted element is inversely proportional to that of *R*-factor. The sample with a small *R*-factor indicates a large hexagonal ordering, suggesting that this sample has well-ordered hexagonal structure. This sample has a large first discharge capacity. The variations of cation mixing and hexagonal ordering with the substituted

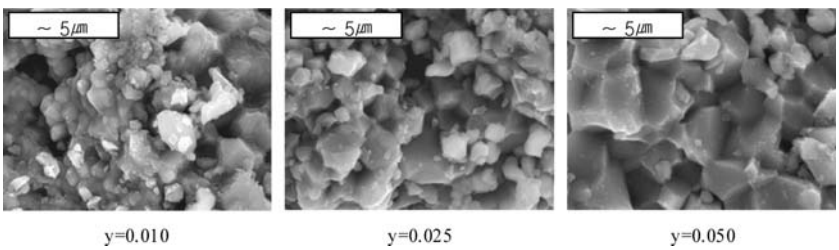

Fig. 8. SEM photographs of $LiNi_{1-y}Tl_yO_2$ (y = 0.01, 0.025 and 0.05) calcined at 750 °C for 36 h.

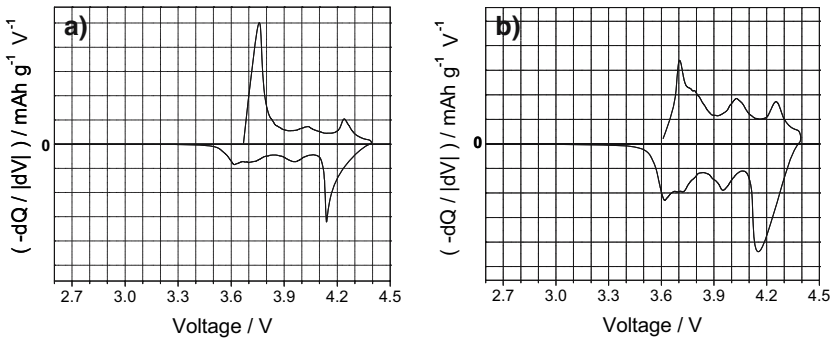

Fig. 10. dQ/|dV| vs. Voltage for $LiNi_{0.975}Ga_{0.025}O_2$ synthesized by the combustion method; (a) the first cycle and (b) the second cycle.

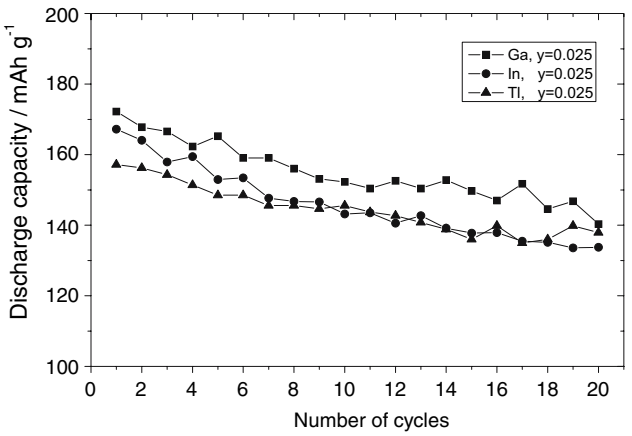

Fig. 11. Variations of discharge capacity at 0.1 C with the number of cycles for $LiNi_{0.975}M_{0.025}O_2$ (M = Ga, In and Tl) synthesized by the combustion method.

element lead to the behavior of the first discharge capacity with the substituted element. Although $LiNi_{0.975}In_{0.025}O_2$ has a small amount of impurity ($LiInO_2$), it has higher first discharge capacity than $LiNi_{0.975}Tl_{0.025}O_2$. Less cation mixing and larger hexagonal ordering of $LiNi_{0.975}In_{0.025}O_2$, compared with $LiNi_{0.975}Tl_{0.02}5O_2$, are considered to lead to this result. The degradation rate of discharge capacity is smallest when M = Tl.

4. Conclusions

$LiNi_{1-y}M_yO_2$ (M = Ga, In and Tl, y = 0.010, 0.025 and 0.050) with small y synthesized by the combustion method by calcining in O_2 stream at 750 °C for 36 h had the $R\bar{3}m$ structure, and $LiNi_{1-y}In_yO_2$ contained $LiInO_2$

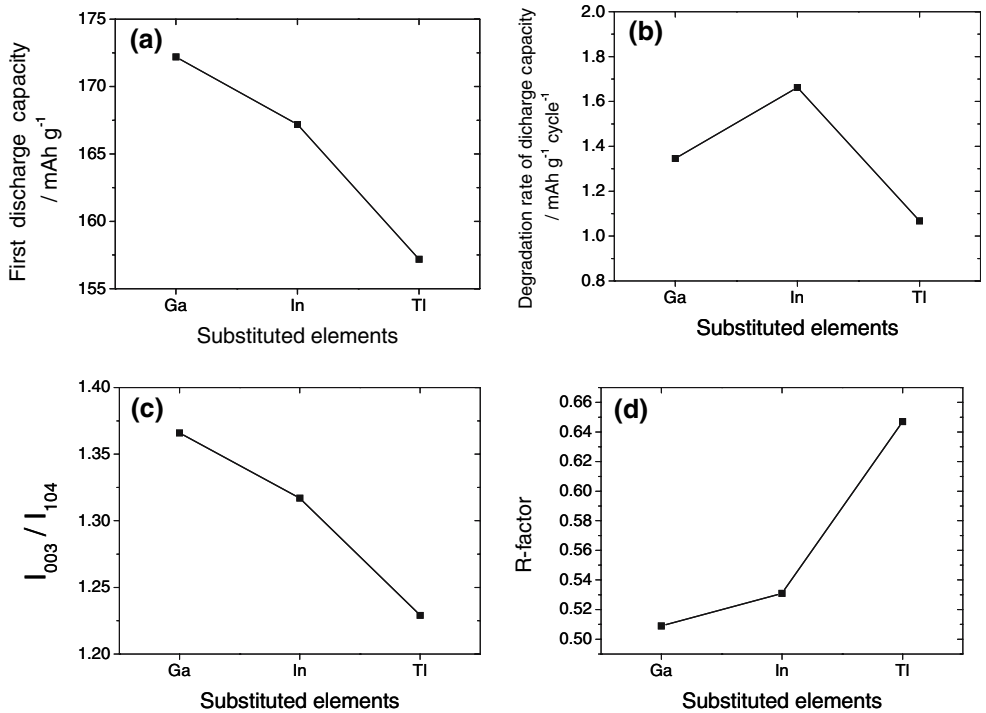

Fig. 12. Variations, with the substituted element, of (a) the first discharge capacity, (b) the degradation rate of discharge capacity, (c) I_{003}/I_{104} and (d) *R*-factor for $LiNi_{0.975}M_{0.025}O_2$ (M = Ga, In and Tl) synthesized by the combustion method.

phase as an impurity. Among $LiNi_{1-y}Ga_yO_2$ the sample with $y = 0.025$ had a relatively large first discharge capacity (172.2 mAh g^{-1}) and relatively good cycling performance. Among $LiNi_{1-y}In_yO_2$ the sample with $y = 0.010$ showed the largest first discharge capacity (167.7 mAh g^{-1}) and larger discharge capacities from $n = 2$ to $n = 20$. Among $LiNi_{1-y}Tl_yO_2$ the sample with $y = 0.025$ had the largest first discharge capacity (157.2 mAh g^{-1}) and the largest discharge capacities from $n = 2$ to $n = 20$. Among $LiNi_{1-y}M_yO_2$ (M = Ga, In and Tl, $y = 0.010$, 0.025 and 0.050), $LaNi_{0.975}Ga_{0.025}O_2$ with a relatively large first discharge capacity (172.2 mAh g^{-1}) and good cycling performance (discharge capacity 140.3 mAh g^{-1} at $n = 20$) exhibited the best electrochemical properties. For $LiNi_{0.975}M_{0.025}O_2$ (M = Ga, In and Tl), the first discharge capacity decreased in the order of the substituted enement Ga, In and Tl. The variations of cation mixing and hexagonal ordering with the substituted element (decrease in I_{003}/I_{104} and increase in *R*-factor from M = Ga through M = Tl) are considered to lead to the behavior of the first discharge capacity with the substituted element. $LiNi_{0.975}Tl_{0.025}O_2$ had the smallest discharge capacity degradation rate.

Acknowledgement

This work was supported by grant No. R01–2003–000–10325–0 from the Basic Research Program of the Korea Science & Engineering Foundation.

References

1. J.M. Tarascon, E. Wang, F.K. Shokoohi, W.R. McKinnon S. Colson, *J. Electrochem. Soc.* **138** (1991) 2859.
2. A.R. Armstrong and P.G. Bruce, *Lett. Nature* **381** (1996) 499.
3. D.S. Ahn and M.Y. Song, *J. Electrochem. Soc.* **147**(3) (2000) 874.
4. K. Ozawa, *Solid State Ionics* **69** (1994) 212.
5. R. Alcátara, P. Lavela, J.L. Tirado, R. Stoyanova and E. Zhecheva, *J. Solid State Chem.* **134** (1997) 265.
6. Z.S. Peng, C.R. Wan and C.Y. Jiang, *J. Power Sources* **72** (1998) 215.
7. J.R. Dahn, U. von Sacken and C.A. Michal, *Solid State Ionics* **44** (1990) 87.
8. J.R. Dahn, U von Sacken, M.W. Juzkow and H. Al-Janaby, *J. Electrochem. Soc.* **138** (1991) 2207.
9. A. Marini, V. Massarotti, V. Berbenni, D. Capsoni, R. Riccardi, E. Antolini and B. Passalacqua, *Solid State Ionics* **45** (1991) 143.
10. W. Ebner, D. Fouchard and L. Xie, *Solid State Ionics* **69** (1994) 238.
11. R. Kanno, H. Kubo, Y. Kawamoto, T. Kamiyama, F. Izumi, Y. Takeda and M. Takano, *J. Solid State Chem.* **110** (1994) 216.
12. A. Hirano, R. Kanno, Y. Kawamoto, Y. Takeda, K. Yamaura, M. Takano, K. Ohyama, M. Ohashi and Y. Yamaguchi, *Solid State Ionics* **78** (1995) 123.
13. A. Rougier, P. Gravereau and C. Delmas, *J. Electrochem. Soc.* **143** (1996) 1168.
14. H. Arai, S. Okada, Y. Sakurai and J. Yamaki, *Solid State Ionics* **95** (1997) 275.
15. M.Y. Song and R. Lee, *J. Power Sources* **111**(1) (2002) 97.
16. M.Y. Song, I.K. Kwon, H.U. Kim, S.B. Shim and D.R. Mumm, *J. Appl. Electrochem.* **36** (2006) 801.
17. D. Caurant, N. Baffier, B. Garcia and J.P. Pereira-Ramos, *Solid State Ionics* **91** (1996) 45.
18. A. Rougier, I. Saadoune, P. Gravereau, P. Willmann and C. Delmas, *Solid State Ionics* **90** (1996) 83.
19. K.K. Lee and K.B. Kim, *J. Electrochem. Soc.* **147**(5) (2000) 1709.
20. G.T.-K. Fey, W.H. Yo and Y.C. Chang, *J. Power Sources* **105** (2002) 82.
21. M.Y. Song, I.H. Kwon and H.U. Kim, *J. Appl. Electrochem.* **35** (2005) 1073.
22. M. Guilmard, A. Rougier, M. Grune, L. Croguennec and C. Delmas, *J. Power Sources* **115** (2003) 305.
23. M.Y. Song, R. Lee and I.H. Kwon, *Solid state Ionics* **156** (2003) 319.
24. T. Amriou, A. Sayede, B. Khelifa, C. Mathieu and H. Aourag, *J. Power Sources* **130** (2004) 213.
25. E. Shinova, E. Zhecheva, R. Stoyanova, G.D. Bromiley, R. Alcántara and J.L. Tirado, *J. Solid State Chem.* **178** (2005) 2692.
26. Y. Gao, M.V. Yakovleva and W.B. Ebner, *Electrochem. Soc.* **142** (1995) 702.
27. S.H. Chang, S.G. Kang, S.W. Song, J.B. Yoon and J.H. Choy, *Solid State Ionics* **86–88** (1996) 171.
28. Y. Gao, M.V. Yakovleva and W.B. Ebner, *Electrochem. Solid-state lett.* **1** (1998) 117.
29. J. Kim and K. Amine, *Electrochem. Commun.* **3** (2001) 52.
30. J. Kim and K. Amine, *J. Power Sources* **104** (2002) 33.
31. Y. Nishida, K. Nakane and T. Stoh, *J. Power Sources* **68** (1997) 561.
32. M. Guilmard, L. Croguennec and C. Delmas, *J. Electrochem. Soc.* **150**((10) (2003) A1287.
33. M.Y. Song and D.S. Ahn, *Solid State Ionics* **112** (1998) 245.
34. J.N. Reimers, E. Rossen, C.D. Jones and J.R. Dahn, *Solid State Ionics* **61** (1993) 335.
35. R. Kanno, T. Shirane, Y. Inaba and Y. Kawamoto, *J. Power Sources* **68** (1997) 145.
36. G. Prado, E. Suard, L. Fournes and C. Delmas, *J. Mater. Chem.* **10** (2000) 2553.
37. S.R. Jain, K.C. Adiga and V. Pai Verneker, *Combust. Flame* **40** (1981) 71.
38. Y. Zhang and G.C. Stangle, *J. Mater. Res.* **9** (1994) 1997.
39. T. Ohzuku, A. Ueda and M. Nagayama, *J. Electrochem. Soc.* **140** (1993) 1862.
40. H. Arai, S. Okada, H. Ohtsuka, M. Ichimura and J. Yamaki, *Solid State Ionics* **80** (1995) 261.
41. W. Li, J.N. Reimers and J.R. Dahn, *Solid State Ionics* **67** (1993) 123.
42. Q. Zhong and U. von Sacken, *J. Power Sources* **54** (1995) 221.